Analysis of the Godunov Based Hybrid Model for Ramp Metering and Robust Feedback Control Design

Pushkin Kachroo, *Senior Member, IEEE,* Lillian Ratliff, *Student Member, IEEE,* and Shankar Sastry, *Fellow, IEEE*

Abstract—This paper presents the detailed analysis of a Godunov approximation based dynamics model for an isolated traffic ramp metering problem. The model for the system is based on a Godunov numerical scheme so that the lumped parameter approximation retains the weak solution shock and rarefaction wave properties exhibited by the distributed model. The paper explicitly considers uncertainty in the system parameters and shows how to design controllers that are robust to those uncertainties. Simulations are performed to show the effectiveness of the proposed control law.

Index Terms—Ramp Metering, Traffic Control, Adaptive, Feedback

I. INTRODUCTION

R AMP metering is a way to influence the amount of traffic on a highway by controlling the inflow from connected streets. Ramp metering technique has been around for more than 45 years, see [1], [2], [3], and [4]. A general overview of ramp metering is provided in the Traffic Control Systems Handbook [5]. Some researchers have used optimization based methods for ramp metering such as [6], [7], and [8]. Many researchers (see [9], and [10]) have used simulations to assess the effectiveness of ramp metering methods. One of the first feedback control theory based control law was ALINEA which is built on linearization and time discretization model of the ramp [11]. Intelligent control methods such as fuzzy logic based controller is presented in [12], and a neural network based in [13]. A decentralized ramp control design is presented in [14]. Many countries, such as U.S.A [15], France [16], Italy [17], Germany [18], New Zealand [19], U.K. [20], and Netherlands [21] utilize ramps for controlling traffic flows. Nonlinear lumped parameter model based feedback control is detailed in [22]. Various model formulations such as the distributed model, lumped model, and their continuous and discrete time versions are shown in [23] and [24]. Recently, there has been interest in developing ramp meter control using the distributed LWR model directly (such as in [22] and [25]. The work in [22] is based on feedback linearization in the distributed setting, while the methodology in [25] uses adjoint based optimization. The current paper deals with designing the control in the lumped parameter setting.

P. Kachroo is with the Department of Electrical and Computer Engineering,at UNLV, and also a visiting Professor at University of California Berkeley e-mail: (see http://faculty.unlv.edu/pushkin/).

L. Ratliff and S. Sastry are with University of California Berkeley.

Godunov's numerical method based discretization has been used to model the ramp metering problem in [26], [27], and [28]. The paper [26] used feedback linearization assuming perfect knowledge of the model by the controller, paper [27] used sliding mode control for the same problem, and the paper [28] deals with the problem with uncertain free flow speed using sliding mode control.

In this paper we study the impact of the uncertainty in the jam density parameter to the control design. The Godunov based model renders the system as a hybrid system with discrete states, where in each state there are different inflow and outflow conditions. When there are no uncertainties, then the controller knows exactly which discrete state the system is in, and hence the nonlinear dynamics can be cancelled such as in feedback linearization as in [26] and sliding mode control as in [27]. Even in the case of uncertainty in the freeflow speed parameter, the discrete state is still known completely, and the uncertainty of the parameter can be handled using sliding mode control as in reference [28]. With uncertainty in the jam density parameter, the controller will have to perform hybrid state estimation for the discrete state and then apply the appropriate control law for the estimated discrete state. However, if flow and traffic density sensors are available then the design does not have to explicitly deal with the discrete state estimation. Depending on what precise sensors are available, different factors in the design come into play. For instance if only occupancy sensors are used, then that data has to be processed to produce traffic density values. Errors in the sensor values have to be accounted for either by using signal processing or with explicit control design to handle those. A camera based sensor can provide instantaneous traffic density, and multilane radar based sensors provide information on multiple variables. This paper presents a detailed analysis of the Godunov based dynamics of the isolated ramp metering problem. It shows details of the discrete transitions for the dynamics. Following that, the paper addresses control design for the system with and without uncertainties and for various possible scenarios for

II. BACKGROUND

Ramp meters are designed to control the inflow into the highway so that the highway can be maintained at better flow conditions. Ramp metering can be deployed based on time of day schedules, or it can also be deployed based on sensor measurements and feedback control. Figure 1 illustrates an
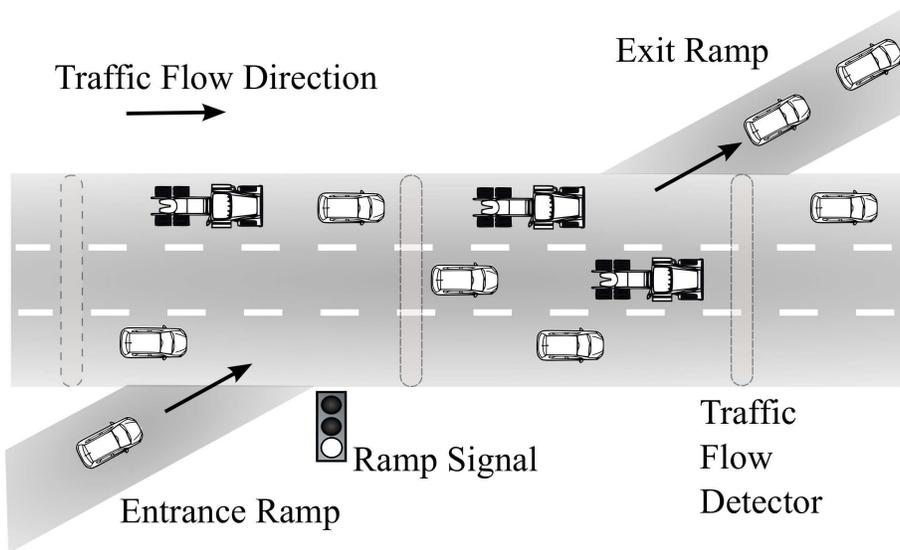
Fig. 1. Ramp Metering

isolated ramp that can be controlled by metering to effect the traffic conditions on the highway.

Many different types of dynamics have been used to design control laws for ramps. The model used in [1] is a simple inflow outflow balanced steady state model. The model used in [11] is a linearized discrete time model for the ramp dynamics. Many lumped parameter based and also distributed models have been studied in [22]. The lumped parameter models used previously had a flaw in that they did not produce vanishing viscosity weak solutions in the limit. In order to address this, enhanced models have been used in [26], [27], and [28]. We present the same dynamics as in these three references below. Following that uncertainty in the jam density will be considered in this paper, and a methodology to deal with that. The hybrid estimation scheme for the design will be presented below followed by simulation results.

III. MATHEMATICAL MODEL

The classic LWR (Lighthill-Whitham-Richards) model is a macroscopic one-dimensional traffic model named after the authors in [29] and [30]. The dynamic evolution equation in that model is the one shown in Equation (1).

$$\frac{\partial}{\partial t}\rho(t,x) + \frac{\partial}{\partial x}f(t,x) = 0 \tag{1}$$

Here, ρ is the traffic density and f, the product of traffic density and the traffic speed v, is the flux, i.e. $f = \rho v$. Many models linking traffic density to traffic speed have been proposed. A linear relationship between traffic density and traffic speed is used in the Greenshield's model (see [31]).

$$v(\rho) = v_f(1 - \frac{\rho}{\rho_m}) \tag{2}$$

where v_f is the free flow speed and ρ_m is the maximum possible density. Free flow speed is the traffic speed when there is no traffic, i.e. when the traffic density is zero. This is the maximum speed possible in this model. The traffic jam density is the density at which there is a traffic jam and which causes the traffic speed to be equal to zero.

Space discretization of Equation (1) for the ramp metering is presented in Figure 2. Here, the ramp inflow into the freeway is given by $u(t)$.
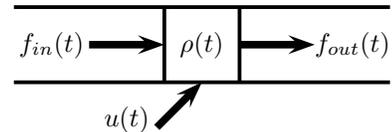

Fig. 2. Discretized Model

Assuming unit length for the section, the ordinary differential equation (ODE) model from the figure for the ramp metering, is given by

$$\frac{d\rho(t)}{dt} = f_{in}(t) + u(t) - f_{out}(t) \tag{3}$$

The inflow term f_{in} is the traffic flowing into the entering section. The control variable u is the inflow from the ramp that we are trying to control. The outflow traffic using Greenshields model is given by

$$f_{out}(t) = v_f\rho(t)(1 - \frac{\rho(t)}{\rho_m}) \tag{4}$$

Insight into the system evolution can be obtained by studying the characteristics emanating from an initial value problem for a Riemann's problem where the upstream traffic density is lower (see [32], [33], and [34]). Figure 3 shows the characteristics of traffic where the initial traffic data is shown on the x-axis, where the the traffic density is piecewise constant. The middle section has the jam density ρ_m, the upstream has a lower density ρ_0 and the downstream has zero

density. As time increases, as shown on the y-axis, the shock wave travels upstream and at the same time the jam dissipates as a rarefaction onto the downstream.
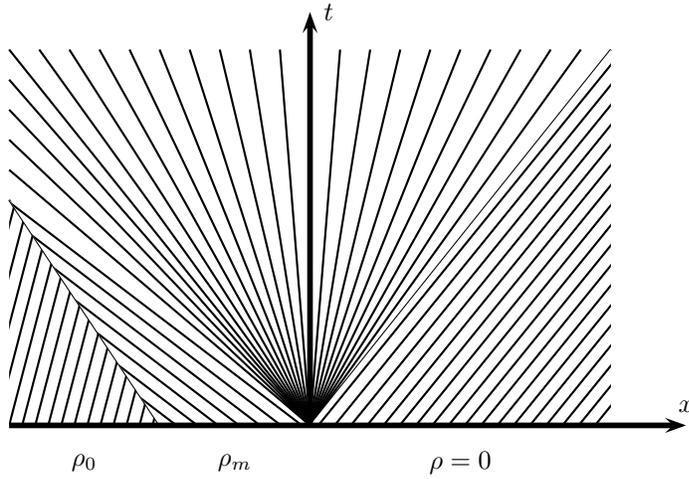

Fig. 3. Traffic Characteristics

We use the Godunov model as our nominal model for the control design.

A. Godunov based Model

The Godunov method is based on solving the Riemann problem where the initial condition is a piecewise constant function with two values ρ_ℓ and ρ_r for the upstream (left) and downstream (right) densities (see [35]). From the junction of the two densities either a shockwave or a rarefaction wave can emanate. A shockwave develops if $f'(\rho_\ell) > f'(\rho_r)$ (see [36]).
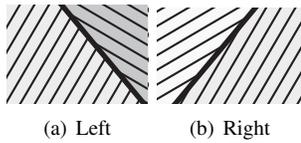

(a) Left   (b) Right

Fig. 4. Shockwaves moving Upstream (left) and Downstream (right)

The speed of the shockwave is given by Equation (5). In this equation, $x_s(t)$ is the position of the shockwave as a funcction of time. If the shock speed is positive then the inflow at junction between the two traffic densities will be a function of upstream traffic density, whereas if the shock speed is negative then the inflow at junction between the two traffic densities will be a function of downstream traffic density.

$$s = \frac{dx_s(t)}{dt} = \frac{[f(\rho_\ell) - f(\rho_r)]}{\rho_\ell - \rho_r} \qquad (5)$$

A rarefaction develops if $f'(\rho_\ell) < f'(\rho_r)$. The rarefaction can be entirely to the left, or to the right or in the middle.

The analysis of the shockwave and rarefaction conditions gives us the Godunov based ODE model for traffic. The ODE
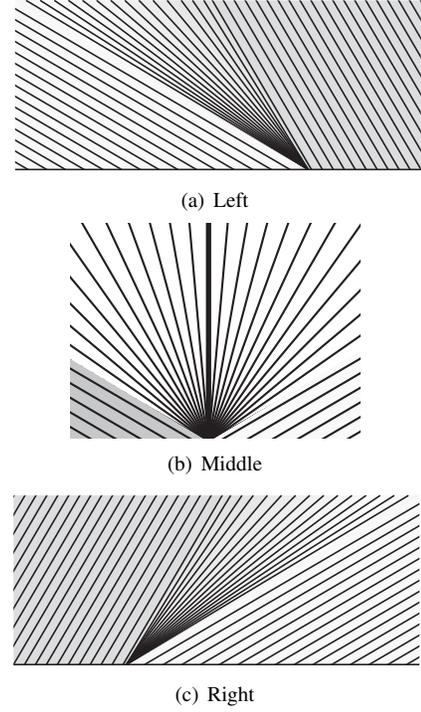

(a) Left

(b) Middle

(c) Right

Fig. 5. Rarefaction Solution

for this method is derived from the conservation law, and is give by Equation (6), where we have assumed unit length for the section. To derive the rest of the model, please consider Figure 6.

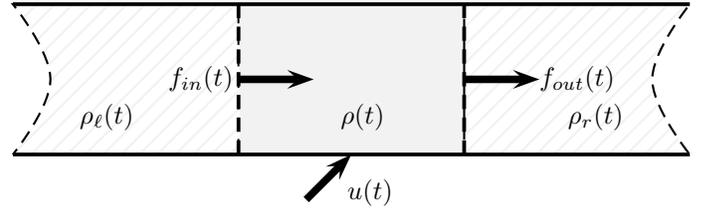$$\frac{d\rho(t)}{dt} = f_{in}(t) - f_{out}(t) + u(t) \qquad (6)$$

Fig. 6. Godunov Dynamics

Now, the inflow $f_{in}(t)$ will be a function of upstream density ρ_ℓ and downstream density ρ_r. Here upstream and downstream are with respect to the left junction. Hence we have the relationship given by Equation (7) where we have used the function $F(\cdot, \cdot)$ that will be obtained from the Godunov method.

$$f_{in}(t) = F(\rho_\ell, \rho) \qquad (7)$$

Similarly, for the right junction, the outflow $f_{out}(t)$ is given by Equation (8).

$$f_{out}(t) = F(\rho, \rho_r) \tag{8}$$

The function $F(\rho_\ell, \rho_r)$ in terms of its arguments is given by the Godunov method as follows (see section 13.5, pages 143-145 [35]).

$$F(\rho_\ell, \rho_r) = f(\rho^*(\rho_\ell, \rho_r)) \tag{9}$$

Here, the flow-dictating density ρ^* is obtained from the following (see [35]):

1) $f'(\rho_\ell), f'(\rho_r) \geq 0 \Rightarrow \rho^* = \rho_\ell$
2) $f'(\rho_\ell), f'(\rho_r) \leq 0 \Rightarrow \rho^* = \rho_r$
3) $f'(\rho_\ell) \geq 0 \geq f'(\rho_r) \Rightarrow \rho^* = \rho_\ell$ if $s > 0$, otherwise $\rho^* = \rho_r$
4) $f'(\rho_\ell) < 0 < f'(\rho_r) \Rightarrow \rho^* = \rho_s$

Here, ρ_s is obtained as the solution to $f'(\rho_s) = 0$.

IV. HYBRID DYNAMICAL MODEL

The ODE model for the ramp metering system can be written as

$$\frac{d\rho(t)}{dt} = F(\rho_\ell, \rho) - F(\rho, \rho_r) + u(t) \tag{10}$$

This is a switched hybrid system (see [37]), where the switching happens autonomously based on the values of ρ_ℓ, ρ, and ρ_r. The function $F(\rho_\ell, \rho)$ can have three distinct values, $f(\rho_\ell)$, $f(\rho)$, or $f(\rho_s)$. Similarly, $F(\rho, \rho_r)$ can have three distinct values. Hence, the dynamics can be written as

$$\frac{d\rho(t)}{dt} = G_q(\rho_\ell, \rho, \rho_r) + u(t) \tag{11}$$

where $q \in \{1, 2, \cdots, 9\}$ and the different G_q functions can be obtained from Equations 9, 10, and 11. In fact, not all the nine states are in fact physically possible in the system. The state size reduction is performed next that shows in fact that $q \in \{1, 2, \cdots, 8\}$.

When in the interface between ρ_ℓ and ρ, the flow is dictated by ρ_ℓ, it can happen because of either the shock travelling to the right as shown in Figure 4(b), or the rarefaction being entirely to the right as shown in Figure 5(c). In this case, the interface between ρ and ρ_r can either have a shock to the left or right, or a rarefaction wave to the left or right, or a transonic wave. In either case, its flow can be dictated by its left or right density, and also by the transonic case. When the flow on the left interface is dictated by the density on its right, it can happen because of either the shock travelling to the left as shown in Figure 4(a) , or the rarefaction being entirely to the left as shown in Figure 5(a). In this case, a transonic wave or a shock travelling to the left can be formed on the right interface, but not a shock moving to its right. In the case of the transonic wave on the left interface, we can have a shock to right or left, or a rarefaction to the right, but no transonic wave on the right interface. We can also have a case where we have transonic wave at both interfaces. In summary, we have a total of eight discrete states instead of nine.

We will use a specific ordered notation for each of the eight states. We will use L at an interface to signify the case where
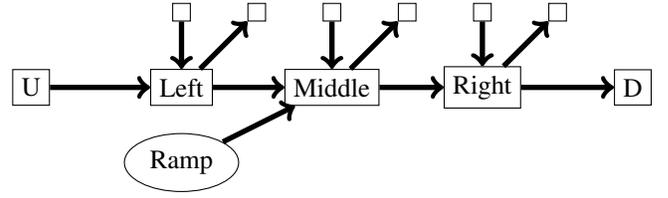

Fig. 7. Ramp Configuration Diagram

the shock or the rarefaction is entirely to the left. In other words the flow at that interface is due to the flow of the right hand side traffic density. Similarly, we will use R at an interface to signify the case where the shock or the rarefaction is entirely to the right. In other words the flow at that interface is due to the flow of the left hand side traffic density. Finally, we will use the symbol $*$ to indicate the transonic wave at that interface. The ordered pair (a, b) where $a \in \{L, R, *\}$ and $b \in \{L, R, *\}$ gives the discrete state of the system. Hence if the discrete state of the system $q \in Q$, the discrete state space, we have

$$Q = \{(L, L), (L, *), (R, L), (R, R), (R, *), (*, L),$$
$$(*, R), (*, *)\} \tag{12}$$

We will also use a similar notation to specify which category in each discrete state the system is in. For instance if the system is in (L, L), it could be in (s, s) which means shock at both edges, or in (s, r) which means shock at left, and rarefaction on the right, etc. Hence, this notation to specify the *sub-states*, we use the ordered pair (a, b) where $a \in \{s, r, *\}$ and $b \in \{s, r, *\}$ gives the discrete sub-state of the state of the system. In fact if we represent the discrete state of the system as X, then the various states would be represented by terms like $((L, L), (s, s))$, $((L, L), (s, r))$ etc. In fact $Q = X/\sim$, where the equivalence relationship is essentially indicated by the sub-states just discussed above.

A. Transitions in the Hybrid Dynamical Model

Next we will study the transitions between the eight different states. We will analyze what transitions are possible between different states with control variable applying non-impulsive input. We will study the transitions for the states in details. In order to do that we will study all the different cases within the different states that occur as well.

The transitions that are possible for a ramp depend on the existence of other entrance and exit ramps at various locations. Figure 7 shows the situation where the left, middle, and the right sections each have additional ramps. The letters U and D stand for the upstream and downstream links on the freeway. This means that the traffic density in each section can be independently increased or decreased. Hence transitions from any of the eight states to all other states are possible. This scenario is shown in Figure 8.

From now on, we will consider the case as shown in Figure 9. Here the only way to change density apart from the ramp
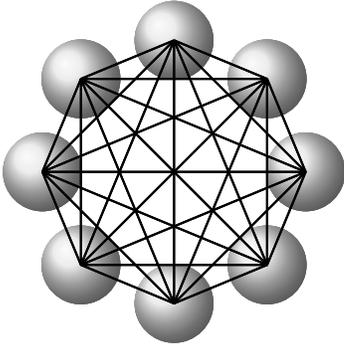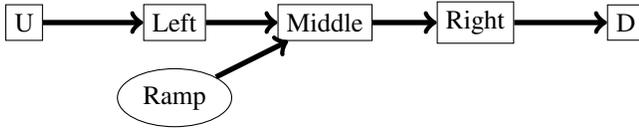
Fig. 8. All Transitions

Fig. 9. Ramp Configuration Diagram with a Single Ramp

inflow is via the left most and right most link interactions. We will consider various different cases for this scenario next.

The transition analysis depends on the following two principles of our modeling:

1) Conservation law is followed at links using continuous time, and
2) the flow at the interface in between links follows the Godunov characteristics conditions.

The key point in figuring out the transition dynamics is also the fact that all traffic flows from upstream to downstream are non-negative. Hence for the ramp metering problem of Figure 9, we see that the ramp inflow and inflow from the left link can only help to increase the density in the middle link, and the outflow to the right link can only help to decrease the density. The combined effect of the two decides the transitions. The effect of reducing the traffic density of the middle link is the same as rotating its characteristic counter-clockwise, whereas the effect of increasing the traffic density of the middle link is the same as rotating its characteristic clockwise.

State (L, L) Transition: Here we consider the case when the flow at both intersections is governed by the densities on the right. The characteristics of the density in the middle link has to be negative for this case. The characteristics of the right link will also be negative. The left link however can have negative or positive characteristics. When it is positive though, its flow must be higher than that of the middle link density to create a negative shock. Summarizing:

1) The densities for the middle link and the right link will be in the congested region, i.e. the region from the critical, peak flow density, and jam density.
2) The left density can be in any region, but its flow has to be higher than the one corresponding to the middle link density.

The possible scenarios for the state (L, L) are enumerated below. These four possibilities are shown in Figure 10. The characteristics for these four cases are shown in Figure 11.

Case 1: The middle density is lower than the right link density creating a shock at the right edge. The left edge flow in this case is $f(\rho)$, and the right edge flow is $f(\rho_r)$, and since $f(\rho) > f(\rho_r)$, the density in the middle link will increase.

Case 2: The middle density is higher than the right link density creating a rarefaction wave completely to the left of the right edge. In this case also we see that $f(\rho) > f(\rho_r)$ and therefore, the density in the middle link will increase.

Case 3: The left link density is lower than the middle link density and at the same time its flow is higher than the flow created by the middle link density, creating a shock at the right edge. In this case with ramp closed, $f(\rho) < f(\rho_r)$ and therefore, the density in the middle link will decrease. However, when the ramp inflow is allowed, that inflow can cause the density to increase if $u(t) > f(\rho_r) - f(\rho)$.

Case 4: The left link density is higher than the middle link density creating a rarefaction wave completely to the left of the left edge. In this case as well, just like the previous case, with ramp closed, $f(\rho) < f(\rho_r)$ and therefore, the density in the middle link will decrease. However, when the ramp inflow is allowed, that inflow can cause the density to increase if $u(t) > f(\rho_r) - f(\rho)$.

To study the possible transitions, we first refer to Figure 9 and notice that there are four edges in our problem. We will refer to the edge between the upstream U link and the left link as the upstream edge, the edge between the left link and the middle link as the left edge, the link between the middle and the right link as the right edge, and finally the edge between the right and the downstream D link as the downstream edge. Now, we are ready to establish the transitions.

$(L, L) \to (L, *)$: The path to this transition is as follows. Since the characteristics of the right link have negative slope, the incoming flow to the right link is dictated by its own density. If the density in the downstream has a positive slope, then there is a transonic wave which produces the maximum outflow. This reduces the density in the right link. Another way the density reduction can take place is when the density in the downstream has a negative slope but the slope is less negative than the slope due to the density in the right link. This produces a left leaning rarefaction wave, and that consequently reduces the density in the right link, as it's outflow is higher than its inflow. As this density keeps reducing, the characteristics in the right link start rotating clockwise, eventually becoming positive. If the density in the main link stays in the region so that it's characteristics retain their negative slope, then the right edge reaches the transonic wave condition. Notice that this transition is not a *controlled transition*. What we mean is that the reduction in the density that is needed for the state change can not come solely from the control variable, since the input ramp can only add flow, and can not reduce density consequently.

$(L, L) \to (*, L)$: This transition can only take place when we are in case 3 or case 4. If the left link maintains its density in the region with negative characteristic slope, and the density in the middle link decreases causing a clockwise rotation of its characteristics, the system can switch from (L, L) to $(*, L)$.

$(L, L) \to (R, L)$: This transition can only take place when we are in case 3 where the characteristic slope of the density in

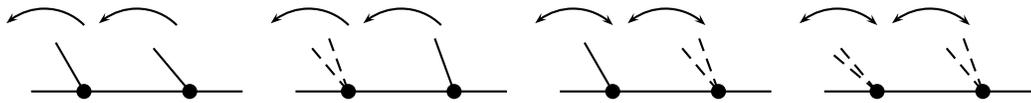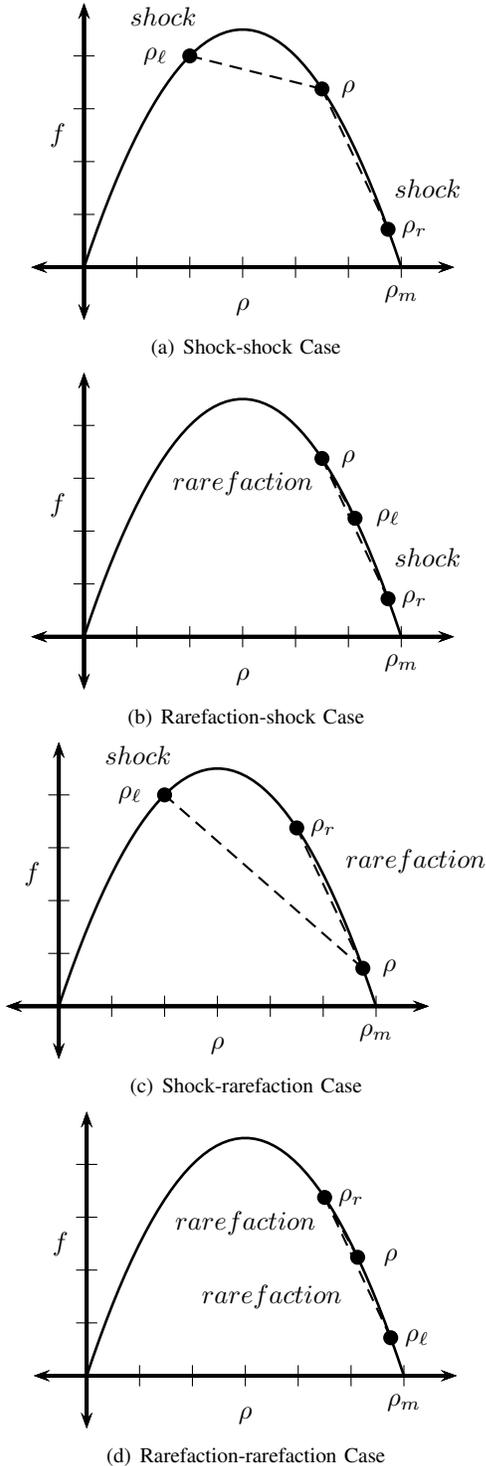Fig. 11.   Traffic Characteristics for (L, L)

(a) Shock-shock Case

(b) Rarefaction-shock Case

(c) Shock-rarefaction Case

(d) Rarefaction-rarefaction Case

Fig. 10.   Four Possibilities for (L, L) State

the left link is positive. In this case, if the left link maintains its density in the region with positive slope maintains slope, and the density in the middle link decreases causing a clockwise rotation of its characteristics, the system can switch from (L, L) to (R, L).

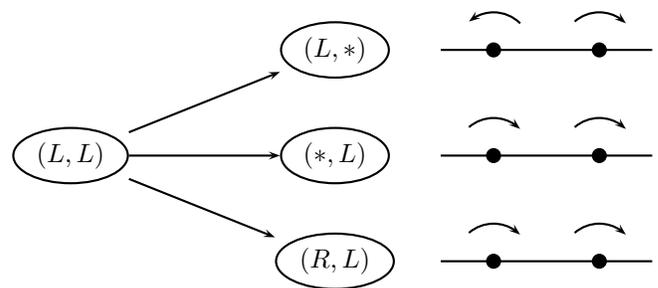These three transitions can be illustrated clearly as shown in Figure 12.

Fig. 12.   Transitions from (L, L)

Similarly, we can draw transitions from all the states and construct the complete transition diagram.

B. Parametric Uncertainty of the Model

In this subsection we will study the impact on the knowledge of the discrete states based on the uncertainties in the free-flow speed and the jam-density parameters of the system. Figure 13 shows the impact the changes in v_f and ρ_m have on the fundamental diagram. The left plot in the figure shows the change in the fundamental diagram, the relationship between the traffic flow and the traffic density being affected by changing the free-flow speed, and the right plot shows the change when just the ρ_m is changed. A careful study of the left plot shows that the change in just the v_f parameter does not change the uncertainty in knowing which discrete state the system is in. This is due to the fact that when the correct density is known, the slope relationship between the slopes at two different densities in terms of their order does not change by the change in v_f. This can be seen if you draw a vertical line at the critical density, which is half of the jam density for this symmetric fundamental diagram. However, this is not true any more in the right plot where the uncertainty is in ρ_m. Now the discrete state is also not known and has to be estimated from the data in real time.

Figure 14 shows the fundamental diagram plots when there is uncertainty is both parameters simultaneously.
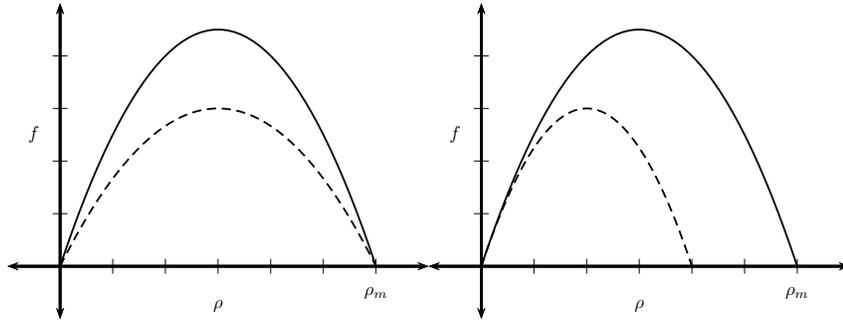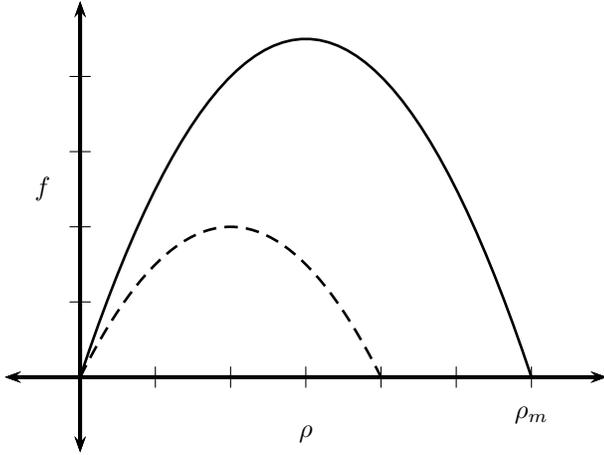
Fig. 13. Fundamental Diagram with Uncertainties

Fig. 14. Fundamental Diagram with Simultaneous Uncertainties

V. ESTIMATION OF THE DISCRETE STATE AND CONTROL DESIGN

The dynamics of the system are

$$\frac{d\rho(t)}{dt} = G_q(\rho_\ell, \rho, \rho_r) + u(t) \tag{13}$$

where

$$G_q(\rho_\ell, \rho, \rho_r) = F(\rho_\ell, \rho) - F(\rho, \rho_r) \tag{14}$$

and

$$F(\rho_\ell, \rho) = f(\rho^*(\rho_\ell, \rho)) \text{ and } F(\rho, \rho_r) = f(\rho^*(\rho, \rho_r)) \tag{15}$$

Here, the flow dictating density is given by Equation (9), and $\rho^*(\rho_1, \rho_2) \in \{\rho_1, \rho_2, \rho_s\}$ where, as shown before, ρ_s is obtained as the solution to $f'(\rho_s) = 0$. As can be seen, ρ_s is the density that provides the maximum flow.

The control design follows a two step procedure. It needs to determine which discrete state the system is in, i.e. to estimate the ρ^* in the left and right edge, and then use an appropriate robust controller for that discrete state. Depending on if the uncertainty is the v_f or ρ_m, we obtain different estimator and control designs. We will present these cases next.

A. No Uncertainties

This case was studied in [26] where a feedback linearization based controller was used, and in [27] where a sliding mode controller was used.

1) Feedback Linearization Based Control: The discrete state of the system in this case is directly known, and then, the following feedback linearization performs cancellation of the non-linearity and produces a exponentially stabilizing feedback law.

$$u(t) = -G_q(\rho_\ell, \rho, \rho_r) - k(\rho - \rho_s), \ k > 0 \tag{16}$$

Certainly, for the actual convergence to take place, there would have to be traffic available at the ramp to increase density when required. Moreover, negative values of the control law are not practically meaningful. Hence, the implemented control law would be

$$u(t) = max(0, -G_q(\rho_\ell, \rho, \rho_r) - k(\rho - \rho_s)), \ k > 0 \tag{17}$$

Let us define the error variable as $e(t) = \rho(t) - \rho_s$, then the closed loop dynamics using control law 16 is given by

$$e(t) + ke(t) = 0, \ k > 0 \tag{18}$$

which gives us the exponentially stable origin as

$$\lim_{t \to \infty} e(t) = 0, \text{ since } e(t) = e^{-kt}e(0) \tag{19}$$

2) Sliding Mode Based Control: For our sliding mode control law, we will take the error variable as the sliding surface variable, i.e. $s(t) = e(t)$. Then we design the control law to obtain the sliding surface attractivity and invariance condition.

$$\frac{1}{2}\frac{d}{dt}s(t)^2 \leq \eta|s(t)|, \ \eta > 0 \tag{20}$$

The control law to obtain this condition that we apply is

$$u(t) = -G_q(\rho_\ell, \rho, \rho_r) - \eta \, \text{sgn}(\rho - \rho_s), \ \eta > 0 \tag{21}$$

B. Uncertainty in v_f

This case is shown in the left subfigure in Figure 13. The flow based on the actual parameters will be shown as $f(\rho)$ and that based on the estimate will be shown as $\hat{f}(\rho)$. We will use v_f to indicate the actual system freeflow speed, and $\hat{v}_f$ as the estimated one. We will consider the parameter error to be bounded, i.e. $|v_f - \hat{v}_f| \leq V$ for a known value of V. Since, the function is assumed known, we have

$$f(\rho) = v_f \rho \left(1 - \frac{\rho}{\rho_m}\right) \tag{22}$$

$$\hat{f}(\rho) = \hat{v}_f \rho \left(1 - \frac{\rho}{\rho_m}\right) = \frac{\hat{v}_f}{v_f} f(\rho) \tag{23}$$

Notice that the term

$$\frac{f(\rho)}{v_f} = \rho \left(1 - \frac{\rho}{\rho_m}\right) \tag{24}$$

does not require the knowledge of v_f, and can be used in the control design.

To understand the implications of the uncertainty in v_f to the estimation of the discrete states, let us study Figure 15.

The left subfigure in Figure 15 shows the case when $\rho_\ell < \rho_r$. Here, the density that dictates the flow is ρ_r, and hence the difference between the actual and the estimated flows is

$$f(\rho^*) - \hat{f}(\rho^*) = (\hat{v}_f - v_f)[\rho \left(1 - \frac{\rho^*}{\rho_m}\right)] = (\hat{v}_f - v_f)\frac{1}{v_f}f(\rho^*) \tag{25}$$

We have a bound on the flow error as

$$|f(\rho^*) - \hat{f}(\rho^*)| = |(\hat{v}_f - v_f)[\rho \left(1 - \frac{\rho^*}{\rho_m}\right)]| \leq V|\frac{1}{v_f}f(\rho^*)| \tag{26}$$

The control law to obtain the condition 20 for this problem with uncertainty in v_f is given by

$$u(t) = -\hat{G}_q(\rho_\ell, \rho, \rho_r) - k \, \text{sgn}(\rho - \rho_s), \ k > 0 \tag{27}$$

where

$$\hat{G}_q(\rho_\ell, \rho, \rho_r) = \hat{F}(\rho_\ell, \rho) - \hat{F}(\rho, \rho_r) \tag{28}$$

and

$$\hat{F}(\rho_\ell, \rho) = \hat{f}(\rho^*(\rho_\ell, \rho)) \text{ and } \hat{F}(\rho, \rho_r) = \hat{f}(\rho^*(\rho, \rho_r)) \tag{29}$$

Now, we derive the bound on error estimate for the function $G(\rho_\ell, \rho, \rho_r)$.

$$|G_q(\rho_\ell, \rho, \rho_r) - \hat{G}_q(\rho_\ell, \rho, \rho_r)| = |(F(\rho_\ell, \rho) - \hat{F}(\rho_\ell, \rho)) - (F(\rho, \rho_r) - \hat{F}(\rho, \rho_r))|$$
$$= |(f(\rho^*(\rho_\ell, \rho)) - \hat{f}(\rho^*(\rho_\ell, \rho))) - (f(\rho^*(\rho, \rho_r)) - \hat{f}(\rho^*(\rho, \rho_r)))|$$
$$\leq V(|\frac{f(\rho_*(\rho_\ell, \rho))}{v_f}| + |\frac{f(\rho_*(\rho, \rho_r))}{v_f}|) \tag{30}$$

Following the method for designing a sliding mode control law for a scalar system with a drift term with bounded uncertainty as shown in chapter 7 of [38], we can take the following gain to obtain the sliding invariance condition.

$$k > V(|\frac{f(\rho_*(\rho_\ell, \rho))}{v_f}| + |\frac{f(\rho_*(\rho, \rho_r))}{v_f}|) + \eta \tag{31}$$

C. Uncertainty in v_f and ρ_m

This case is shown in the right subfigure in Figure 13 where there is uncertainty only in ρ_m and in Figure 14 where both uncertainties are considered simultaneously. To understand the implications of the uncertainty in ρ_m to the estimation of the discrete states, let us study Figure 16.

In the case of the uncertainty in the ρ_m parameter, the fundamental diagram based on the estimated parameter can give the wrong discrete state. For instance, we see in the right sub-figure of Figure 16 that the actual curve shows that the shock speed should be positive, which implies that the flow on the edge should be dictated by the left density, however the curve using the estimated parameter shows a negative shock speed and hence it shows spuriously that the flow at the edge depends on the right density. If the actual and the estimated curves are switched, then we would get the opposite results. There are instances that the discrete state could be correct but obviously the flow errors would still exist. This is the case shown in the right sub-figure in Figure 16, where the actual and the estimated curves both show rarefaction containing the peak flow values, but these values are different for the two curves.

If the controller only has access to three sensors for the three densities ρ_ℓ, ρ, and ρ_r, then the controller would also need to have an explicit discrete state estimator. On the other hand if we have sensors for the left and right edge flows then the need for this explicit estimator is removed. We can clearly use the measurements to know which side of the edge is dictating the flow at an edge. In fact, for the controller, we just directly need these two flow values and the middle density. Many flow detector sensors in fact provide traffic density and traffic flow measurements simultaneously, and hence a controller based on that premise can be easily implemented. When we have uncertainties in both parameters and we have flow sensors, then also we can use the same technique.
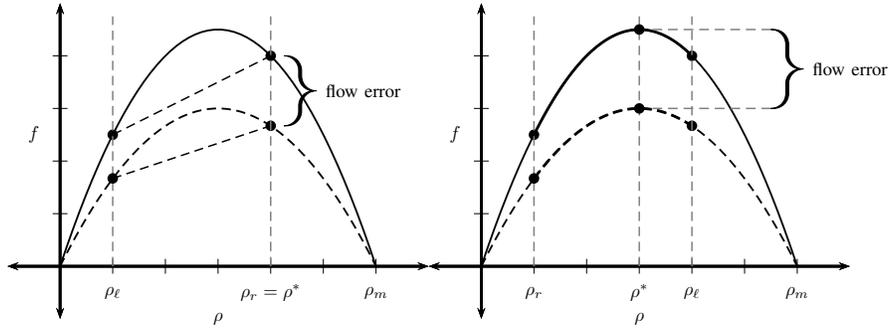
Fig. 15. Discrete States with Uncertain v_f
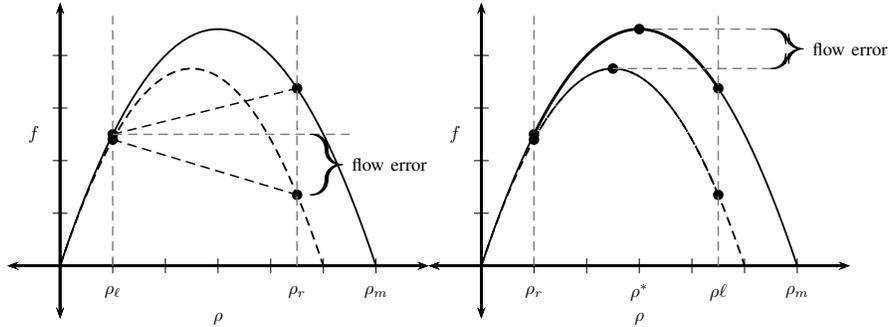
Fig. 16. Discrete States with Uncertain ρ_m

The control law with sensors available for the flows and densities becomes

$$u(t) = -G_q(\rho_\ell, \rho, \rho_r) - k \operatorname{sgn}(\rho - \rho_s), \ k > 0 \qquad (32)$$

In fact, since in this case we can perform complete cancellation, we can even obtain feedback linearization. However, one issue with the result of the controller is that it will lead to a density which is suboptimal, since ρ_s will be $\hat{\rho}_m/2$ and not $\rho_m/2$. To solve this problem, an online parameter estimation scheme can be employed which will convert the controller into a self tuning regulator.

D. Parameter Estimation and Control

The sensing scenario for the ramp control with parameter estimator is shown in Figure 17. The data from the sensors is composed of $\{\rho_\ell, \rho, \rho_r, f_\ell, f_r\}$, where f_ℓ and f_r are the left and right edge flows.

1) Analysis of the Desired System Behavior: To maximize throughput we would want to maximize flow through the mainline. That is accomplished by having a maximum flow out. This flow out must remain constant over time to optimize the performance. This can be accomplished by having
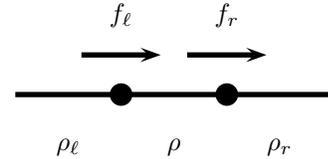

Fig. 17. Sensor Information

$$f(\rho^*(\rho_\ell, \rho)) = f(\rho_s) = f(\rho^*(\rho, \rho_r)) \qquad (33)$$

In order to maintain the transcritical flow at the left edge the characteristics slope in the middle link should have non-negative slope, and in order to have transcritical flow at the right edge the characteristics slope in the middle link should have non-positive slope. This gives a single solution for the middle density to be $\rho = \rho_s$. This can be sustained if the density in the left link has non-positive characteristic slope, and the density on the right has a non-negative characteristic slope.

2) Algorithm Design: In order to build an online estimator for the parameters we need the data pairs $(\rho, f(\rho))$ that can be used to estimate the system parameters. The flow

measurements f_ℓ and f_r are obtained at each sample time, but we need to estimate the best density values that match with these flow values in order to perform recursive estimation at each time step.

One type of estimator can be built using the estimated value of the slope $\partial f/\partial \rho$.

The estimator can be built on the relationship

$$\frac{df}{dt} = \frac{\partial f}{\partial \rho}\frac{d\rho}{dt} \tag{34}$$

The values for df/dt and $d\rho/dt$ can be obtained by using the values of measured flow values at the current and previous sample times, and the corresponding selected density values.

Equation (34) can be viewed as a linear parameter estimation equation

$$y = W\beta \tag{35}$$

where y is a data vector, W a data matrix, and β the parameter vector. The aim is to find the least square estimator for β based on the available data. A recursive least square algorithm for the minimization of the cost given in Equation (36) is given next (see [38]). This can be modified to use only the sign of the estimator. However, in our simulations, we will use the full algorithm for estimation of v_f and ρ_m. The cost to minimize is

$$J = \int_0^t \|y(\tau) - W(\tau)\beta(\tau)\|d\tau \tag{36}$$

The recursive estimator equation is

$$\begin{aligned} \dot{\hat{\beta}}(t) &= -P(t)W'(t)(W(t)\hat{\beta} - y(t)) \\ \dot{P}(t) &= -P(t)W'(t)W(t)P(t) \end{aligned} \tag{37}$$

At any given sampling instant the matching value for a given flow value at the edge can be chosen as follows. If the estimated current $\partial f/\partial \rho$ is positive, we choose density of the left side of the edge to match the edge flow, and if the estimated current $\partial f/\partial \rho$ is negative, we choose density of the right side of the edge to match the edge flow. Now, unless there is in fact an actual shock front at the edge, the densities immediately on the left and right will be different, otherwise, the transition will be smooth. In that case, the traffic sensor data that provides traffic flow and density can be directly used to estimate the traffic parameters using for instance the update law (37).

VI. SIMULATION RESULTS

The simulations that were performed were based on the data obtained from the ramp at the intersection of Interstate I-15 northbound and Tropicana in Las Vegas as shown in Figure 18.

The data from the freeway detector at this location at roadway $id : 59$, and segment $id : 2$ was collected from 6 A.M. to 12 P.M. on a Thursday. The application of the least square estimator to the flow density relationship in order to extract v_f and ρ_m gave us the values of approximately 70

miles/hour, and 86 vehicles/mile respectively. Hence, we use these numbers as our traffic parameters in our simulations.

Now, we apply the control law for the case where the sensor configuration scenario is given by Figure 17, i.e. we have the sensor data $\{\rho_\ell, \rho, \rho_r, f_\ell, f_r\}$. First we assume no uncertainties, and use the control law given by (16). The result of this application is shown in Figure 19. The initial traffic density in the section of 50 vehicles/mile is exponentially decreased to the desired critical value of 43 vehicles/mile. The controller also achieves a steady state value smoothly. The shape of the curves is the results of the first order dynamics that the feedback linearizing control is able to achieve.
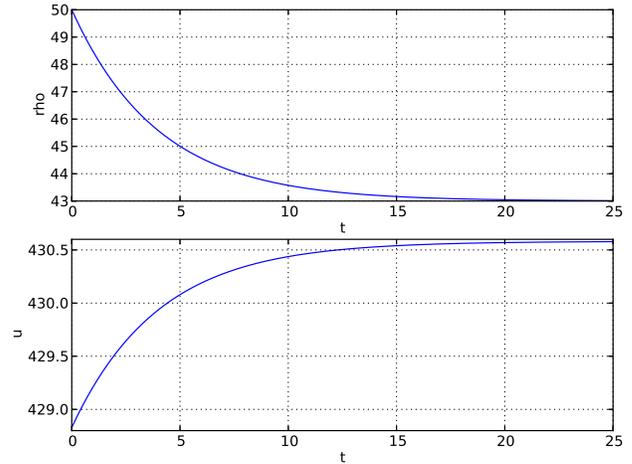

Fig. 19.   Ramp Control with No Uncertainties

Now if we add uncertainty, then the controller will not be able to track the optimal flow corresponding to the critical density. For instance, in our simulation, the estimated jam density for the controller is 76 vehicles/mile as compared to the true value of 86 vehicles/mile. The controller will track the spurious value of 38 instead of 43 as shown in Figure 20.

Now, when we add the adaptation to the parameters so that we use the same controller as before with the difference this time that the target critical density comes from the online estimator equation (37. We observe that the recursive estimator is able to asymptotically track the actual parameter and the control law is able to track the actual critical density to maximize flow as shown in Figure 21.

VII. CONCLUSIONS AND FUTURE WORK

This paper presented a detailed analysis of the Godunov based dynamics for isolated ramp metering problem. The paper then presented various control designs based on different assumptions on sensor configurations and also various scenarios for uncertainties. Finally, the paper presented simulation results for the full sensor case with and without uncertainties including the case of adaptive control law where the controller adapted to the unknown critical density of the system.
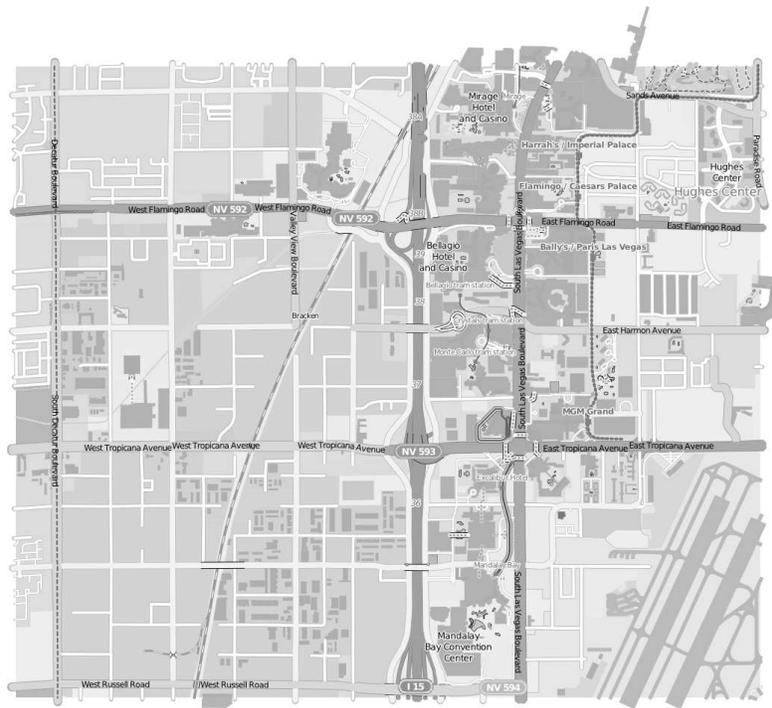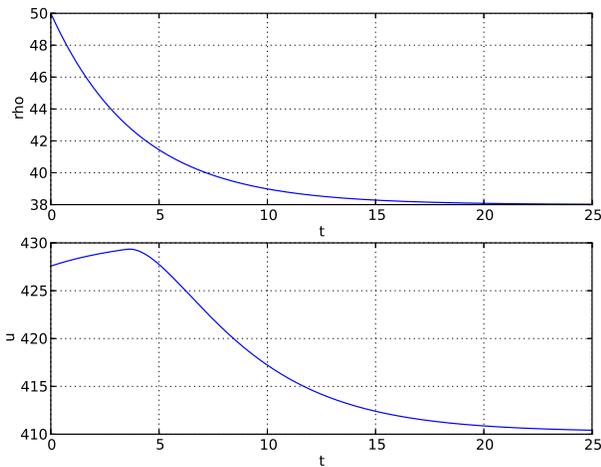
Fig. 18.   Ramp Metering Problem Location

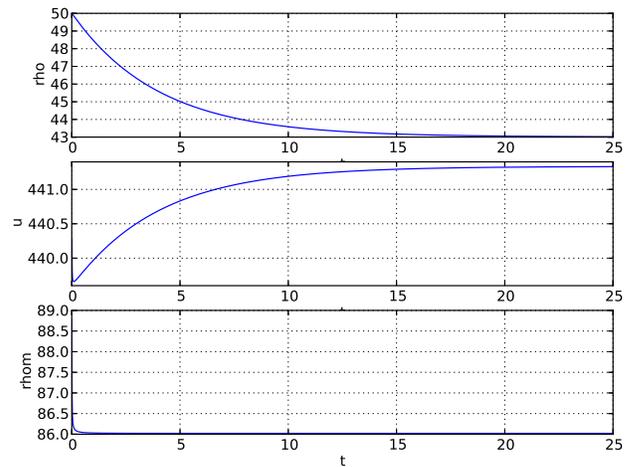Fig. 20.   Ramp Control with Uncertain Parameters

Fig. 21.   Adaptive Ramp Control with Uncertain Parameters

REFERENCES

[1] J. A. Wattleworth, "System demand capacity analysis on the inbound gulf freeway," *Texas Transportation Institute*, vol. 24-8, 1964.

[2] D. R. Drew, "Gap acceptance caharacteristics for ramp freeway surveillance and control," *Texas Transportation Institute*, vol. 24-12, 1965.

[3] C. Pinnell, D. R. Drew, W. R. McCasland, and J. A. Wattleworth, "Inbound gulf freeway ramp control study i," *Texas Transportation Institute*, vol. 24-10, 1965.

[4] ——, "Inbound gulf freeway ramp control study ii," *Texas Transportation Institute*, vol. 24-10, 1965.

[5] ITE, "Traffic control systems handbook," *Institute of Transportation Engineers*, vol. 4.14-4.40, 1996.

[6] L. S. Yuan and J. B. Kreer, "Adjustment of freeway ramp metering rates to balance entrance ramp queues," *Transportation Research*, vol. 5, pp. 127–133, 1971.

[7] J. A. Wattleworth and D. S. Berry, "Peak period control of a freeway system - some theoretical investigations," *Highway Research Record*, vol. 89, pp. 1–25, 1964.

[8] A. D. May, "Optimization techniques applied to improving freeway operations," *Transportation Research Record*, vol. 495, pp. 75–91, 1965.

[9] B. Hellinga and M. V. Aerde, "Examining the potential of using ramp metering as a component of an atms," *Transportation Research Record*, vol. 1494, pp. 75–83, 1995.

[10] H. Zhang, S. Ritchie, and W. Recker, "On the optimal ramp control problem: When does ramp metering work?" *Transportation Research Board Annual Conference*, 1995.

[11] M. Papageorgiou, H. S. Habib, and J. M. Blosseville, "Alinea: A local feedback control law for on-ramp metering," *Transportation Research*

Record, vol. 1320, pp. 58–64, 1991.

[12] L. L. Chen, A. D. May, and D. M. Auslander, "Freeway ramp control using fuzzy set theory for inexact reasoning," *Transportation Research A*, vol. 24, no. 1, pp. 15–25, 1990.

[13] N. B. Goldstein and K. S. P. Kumar, "A decentralized control strategy for freeway regulation," *Transportation Research B*, vol. 16B, no. 4, pp. 279–290, 1982.

[14] H. Zhang, S. Ritchie, and Z. Lo, "A local neural network controller for freeway ramp metering," *IFAC Transportation Systems, PRC*, pp. 655–658, 1994.

[15] D. P. Masher, D. W. Ross, P. J. Wong, P. L. Tuan, H. M. Zeidler, and S. Petracek, "Guidelines for design and operation of ramp control systems," *Stanford Research Institute*, 1975.

[16] H. Hadj-Salem, M. M. Davee, J. M. Blosseville, and M. Papageorgiou, "Alinea: Unoutil de regulation dacces isole sur autoroute," *Rapport INRETS 80*, 1988.

[17] R. L. Pera and R. Nenzi, "Tana - an operating surveillance system for highway traffic control," *Proc., Institute of Electrical and Electronics Engineers*, vol. 61, pp. 542–556, 1973.

[18] N. Helleland, W. Joeppen, and P. Reichelt, "Die rampendosierung an der a5 bonn/siegburg der bab 3 in richtung koln," *Strassenverkehrstechnik*, vol. 22, pp. 44–51, 1978.

[19] NN, "Ramp metering in auckland," *Traffic Engineering and Control*, vol. 24, pp. 552–553, 1983.

[20] D. Owens and M. J. Schofield, "Access contr on the m6 motorway: Evaluation of britains first ramp metering scheme," *Traffic Engineering and Control*, vol. 29, pp. 616–623, 1988.

[21] H. Buijn and F. Middelham, "Ramp metering control in the netherlands," *Proc., 3rd IEE International Conf. on Road Traffic Control*, pp. 199–203, 1990.

[22] P. Kachroo and K. Ozbay, *Feedback Ramp Metering for Intelligent Transportations Systems*. Kluwer, 2003.

[23] P. Kachroo, K. Ozbay, S. Kang, and J. A. Burns, "System dynamics and feedback control formulations for real time dynamic traffic routing," *Mathl. Comput. Modelling*, vol. 27, no. 9-11, pp. 27–49, 1998.

[24] P. Kachroo and K. Krishen, "System dynamics and feedback control design formulations for real time ramp metering," *Transactions of the SDPS, Journal of Integrated Design and Process Science*, vol. 4, no. 1, pp. 37–54, 2000.

[25] D. Jacquet, C. C. de Wit, and D. Koenig, "Optimal ramp metering strategy with an extended lwr model: Analysis and computational methods," in *6th IFAC World Congress*, 2005.

[26] N. Shlayan and P. Kachroo, "Feedback ramp metering using godunov method based hybrid model," *ASME Journal of Dynamical Systems, Measurement and Control*, vol. 5, no. 135, 2013.

[27] B. Sharma, D. Kumar, and P. Kachroo, "Robust hybrid feedback control design for ramp metering using sliding mode control," *International Journal of Advanced Research in Computer Science*, vol. 4, no. 9, 2013.

[28] ——, "Robust ramp metering design using sliding mode control of a hybrid dynamical model with functional uncertainties," *International Journal of Advanced Research in Computer and Communication Engineering*, vol. 2, no. 8, 2013.

[29] M. J. Lighthill and G. B. Whitham, "On kinematic waves. i:flow movement in long rivers. ii:a theory of traffic on long crowded roods," in *Proc. Royal Soc.*, no. A229, 1955, pp. 281–345.

[30] P. I. Richards, "Shockwaves on the highway," *Operationa Research*, vol. 4, pp. 42–51, 1956.

[31] B. D. Greenshields, "A study in highway capacity," *Highway Research Board*, vol. 14, p. 458, 1935.

[32] G. B. Whitham, *Linear and Nonlinear Waves*. N.Y.: John Wiley, 1974.

[33] R. Haberman, *Mathematical Models: Mechanical Vibrations, Population Dynamics, and Traffic Flow*. SIAM, 1987.

[34] P. Kachroo, *Pedestrian Dynamics: Mathematical Theory and Evacuation*. CRC, 2009.

[35] R. J. Leveque, *Numerical Methods for Conservation Laws*. Birkhauser, 2005.

[36] P. D. Lax, *Hyperbolic Systems of Conservation Laws and the Mathematical Theory of Shock Waves*. SIAM, 1987.

[37] A. J. van der Schaft and H. Schumacher, *An Introduction to Hybrid Dynamical Systems*. Springer, 1999.

[38] J.-J. E. Slotine, W. Li *et al.*, *Applied nonlinear control*. Prentice hall, 1991.

Pushkin Kachroo is currently a visiting Professor at the University of California at Berkeley working with Professor Shankar Sastry. He is also the Lincy Professor of Transportation in the department of Electrical and Computer Engineering at the University of Nevada Las Vegas (UNLV). He is the director of the Transportation Research Center at UNLV and also the Associate director of the Mendenhall Innovation Program at the Thomas a Hughes College of Engineering at UNLV. He was an Associate Professor at Virginia Tech before he joined UNLV in 2007. He obtained his Ph.D. in Mechanical Engineering from University of California at Berkeley performing research in Vehicle Control in 1993 under Professor Masayoshi Tomizuka, and obtained another Ph.D. in Mathematics from Virginia Tech in Mathematics in the area of hyperbolic system of partial differential equations with applications to Traffic Control and Evacuation under Professor Joseph A. Ball. He has authored 10 books on traffic and vehicle control. He has authored more than 120 publications that include books, research papers, and edited volumes. He has taught about 30 different courses in Virginia Tech in the areas of electrical and computer engineering, and mathematics. Similarly, he also taught 30 different courses at UNLV since 2007. He has graduated more than 35 graduate students, and has been P.I. or Co P.I. on projects worth more than 4 Million Dollars. He was awarded the most outstanding new professor at Virginia Tech, and also has received many teaching awards and certificates, both at Virginia Tech and UNLV. He also received the faculty excellence award from CSUN UNLV in 2011.

Lillian Ratliff is a doctoral student in the EECS department at the University of California at Berkeley. Her B.S. degrees in Electrical Engineering and Mathematics and M.S. degree in Electrical Engineering were from the University of Nevada Las Vegas. She is the recipient of the NSF graduate fellowship. Generally, she is interested in game theory and dynamical systems. In particular, she is examining ways in which games can be decomposed from a structural point of view. It is common in many engineering problems for strategy spaces or player cost functions to be non-convex. In addition, agents may be myopic. These observations motivate the need for a characterization of equilibrium concepts in games that is amenable to computation. Her research explores these concepts from a dynamical systems perspective. She is also interested in applying other tools from economics to engineering problems, such as mechanism design and pricing, for the purpose of behavior modification in games arising in engineering applications such as cyber-physical systems.

Shankar Sastry is the Dean of the College of Engineering at the University of California, Berkeley. He currently holds the Nippon Electronics Corporation (NEC) Distinguished Professorship in the College of Engineering and the Walter A. Haas School of Business. He was elected to the National Academy of Engineering in 2001 and is a recipient of the Donald P. Eckman Award in 1990. Sastry obtained his bachelor degree from Indian Institute of Technology, Bombay (1977), his master and PhD degrees from University of California, Berkeley (1979, 1980, 1981). His PhD advisor was Professor Charles Desoer. He became an Assistant Professor at Massachusetts Institute of Technology (1980-2), Assistant Professor, Associate Professor, and Professor at University of California, Berkeley (1983present).